

Site, Rate, and Mechanism of Photoprotective Quenching in Cyanobacteria

Lijin Tian,[†] Ivo H. M. van Stokkum,[‡] Rob B. M. Koehorst,[†] Aniek Jongerius,[†] Diana Kirilovsky,[§] and Herbert van Amerongen^{†,||,*}

[†]Laboratory of Biophysics, Wageningen University, P.O. Box 8128, 6700 ET, Wageningen, The Netherlands

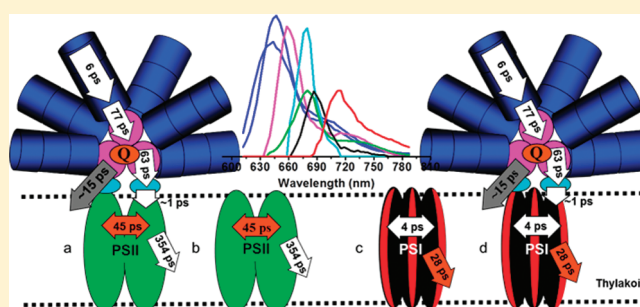
[‡]Biophysics Group, Department of Physics and Astronomy, Faculty of Sciences, VU University, DeBoelelaan 1081, 1081 HV Amsterdam, The Netherlands

[§]Commissariat à l'Energie Atomique, Institut de Biologie et Technologies de Saclay and Centre National de la Recherche Scientifique, 91191 Gif sur Yvette, France

^{||}MicroSpectroscopy Centre, Wageningen University, P.O. Box 8128, 6700 ET, Wageningen, The Netherlands

S Supporting Information

ABSTRACT: In cyanobacteria, activation of the Orange Carotenoid Protein (OCP) by intense blue-green light triggers photoprotective thermal dissipation of excess absorbed energy leading to a decrease (quenching) of fluorescence of the light harvesting phycobilisomes and, concomitantly, of the energy arriving to the reaction centers. Using spectrally resolved picosecond fluorescence, we have studied cells of wild-type *Synechocystis* sp. PCC 6803 and of mutants without and with extra OCP (Δ OCP and OverOCP) both in the unquenched and quenched state. With the use of target analysis, we managed to spectrally resolve seven different pigment pools in the phycobilisomes and photosystems I and II, and to determine the rates of excitation energy transfer between them. In addition, the fraction of quenched phycobilisomes and the rates of charge separation and quenching were resolved. Under our illumination conditions, \sim 72% of the phycobilisomes in OverOCP appeared to be substantially quenched. For wild-type cells, this number was only \sim 29%. It is revealed that upon OCP activation, a bilin chromophore in the core of the phycobilisome, here called APC^Q₆₆₀, with fluorescence maximum at 660 nm becomes an effective quencher that prevents more than 80% of the excitations in the phycobilisome to reach Photosystems I and II. The quenching rate of its excited state is extremely fast, that is, at least (\sim 240 \pm 60 fs)⁻¹. It is concluded that the quenching is most likely caused by charge transfer between APC^Q₆₆₀ and the OCP carotenoid hECN in its activated form.



INTRODUCTION

Too much light can be lethal for photosynthetic organisms and it can for instance induce photo-oxidative damage of the reaction centers (RCs).^{1–3} To protect themselves, plants, algae, and cyanobacteria have evolved protective mechanisms such as nonphotochemical quenching (qE in plants and qE_{cya} in cyanobacteria) to dissipate excess excited-state energy as heat.^{4–6} The occurrence of qE_{cya} in the cyanobacterium *Synechocystis* sp. PCC 6803 (hereafter called *Synechocystis*) and the involvement of the large extra-membrane cyanobacterial antenna, the phycobilisome (PB), was first suggested by El Bissati et al. using strong blue-green light.⁷ Later the action spectrum for qE_{cya} reported by Rakhamberdieva et al.⁸ in a PSII-deficient mutant of *Synechocystis* suggested that blue-green light-activated carotenoids were involved in this mechanism. The involvement of the orange carotenoid protein (OCP) in qE_{cya} was next identified by Wilson et al.,⁹ and it was found that a reversible conformational change of OCP from its inactive orange form (OCP^o) to its active red form

(OCP^r), triggered by blue-green light, is responsible for qE_{cya} .¹⁰ The conformational change is accompanied by a red shift of the absorption maximum of the OCP pigment, 3'hydroxyechinenone (hECN).¹⁰ The activation of the OCP is a very low quantum yield reaction and it is light intensity dependent.¹⁰ Only the OCP^r can bind to the PB and trigger the quenching of the PB.¹¹ Another protein called the Fluorescence Recovery Protein (FRP) is essential to recover the full antenna capacity under low-light conditions after exposure to high irradiance. This protein, by interacting with OCP^r, induces its conversion to OCP^o and helps the detachment of the OCP from the PB.^{11,12} The process of qE_{cya} was investigated in numerous studies during the past few years.^{8–20}

Genes encoding for homologues of the *Synechocystis* OCP are present in most PB-containing cyanobacteria and all these strains

Received: July 23, 2011

Published: October 05, 2011

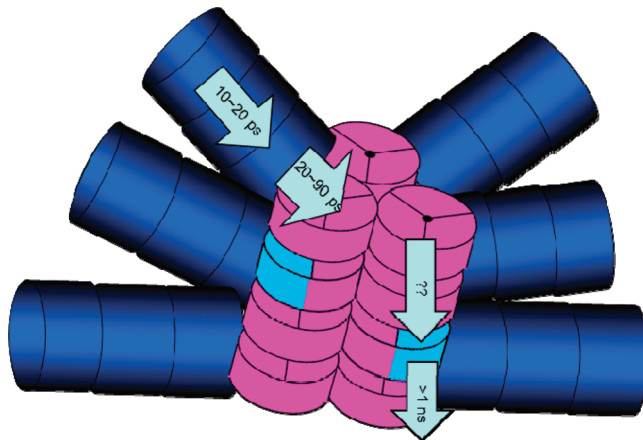


Figure 1. Schematic representation of a *Synechocystis* sp. PCC 6803 PB and previously determined excitation energy transfer times. Dark blue corresponds to C-PC (emitting at 640–650 nm), magenta to APC₆₆₀ (emitting at 660 nm), and cyan to APC₆₈₀ (emitting at ~680 nm). The longest lifetime corresponds to decay to the ground state.

are able to perform qE_{cya}.¹⁷ The quenching efficiency depends on the concentration of OCP. This was demonstrated by studying a mutant overexpressing OCP (OverOCP) that shows more quenching than the wild-type (WT) under the same high-light condition and a mutant not capable of synthesizing OCP (Δ OCP), which shows no quenching at all.^{9,10} Note that in WT cells grown at low- or medium-light conditions the number of OCP's is lower than the number of PBs and presumably not all PBs can be quenched.²¹ Nevertheless, even under these conditions, the qE_{cya} mechanism is photoprotective. The Δ OCP *Synechocystis* mutant is more sensitive to high-light conditions than the WT.⁹ Moreover, cyanobacteria strains containing the OCP are more resistant to photoinhibition than strains lacking the OCP and the qE_{cya} mechanism.¹⁷ Under stress conditions, like iron starvation, the ratio of OCP to phycobilisomes increases inducing a much larger energy and fluorescence quenching rendering the cells more resistant to environmental changes.¹⁸

The fluorescence recovery depends on the FRP to OCP ratio.¹¹ Thus, in WT cells, total fluorescence recovery is reached in only 10 min, while in the overOCP strain, more than 30 min are needed to recover the full antenna capacity at 32 °C. In addition, this reaction is largely temperature dependent: Below 10 °C, almost no recovery is observed.^{10,14}

In *Synechocystis*, the light-harvesting PB contains six C-phycocyanin (C-PC) rods and three allophycocyanin (APC) core cylinders. Each C-PC rod is composed of three hexamer disks with a maximum absorbance at 620 nm and maximum fluorescence at 640–650 nm. Each APC cylinder contains four trimer discs with maximum absorbance at 650 nm. The two APC cylinders which are closest to the membrane contain two trimer discs formed by 3 $\alpha\beta$ APC emitting at 660 nm (APC₆₆₀) and two trimers in which one of the α or the β APC subunits is replaced by a special subunit, ApcD, ApcF, or ApcE, emitting at 680 nm (APC₆₈₀). These terminal emitters function as spectral bridges between PB and photosystems. The third APC cylinder contains only $\alpha\beta$ APC trimers emitting at 660 nm. All of these pigment-proteins (phycobiliproteins) are bound together by several types of linker peptides.^{22–26} PBs form a rather efficient antenna system, funneling more than 90% of the captured energy via

APC₆₈₀ to the lower energy Chls within PSI and PSII, where the photochemical reactions are performed.^{22,23,27,28} A schematic overview of the PB organization is given in Figure 1 together with a global description of previously resolved excitation energy transfer times in *Synechocystis*.^{13,26,29,30}

It is already known that qE_{cya} does not occur in the outer rods that contain the C-PC pigments thanks to various mutant studies.^{8,13,15,18} This has just been confirmed by *in vitro* reconstitution experiments showing that OCP^r can bind to PB containing only the core, thereby completely quenching its fluorescence. In contrast, OCP^r is unable to quench the fluorescence of PB containing only PC rods.¹¹ Therefore, the quenched species should be either an APC₆₆₀ or an APC₆₈₀ pigment in the APC core.^{18,20} It is one of the goals of the present study to find out where exactly in the PB qE_{cya} takes place. The differences in the fluorescence maxima of the various pigments should facilitate the analysis of the ultrafast fluorescence data sets and enable the identification of the quenching site.

qE_{cya} is accompanied by a spectral and conformational change of the carotenoid hECN bound to OCP but it is unknown what the molecular quenching mechanism is. By comparing the spectrally resolved picosecond fluorescence kinetics in the presence and absence of qE_{cya}, we intend to determine the rate of quenching which should then hopefully shed light on the underlying physical mechanism, which is also still unknown.

We have performed picosecond fluorescence measurements on *Synechocystis* WT cells and cells of the OverOCP and Δ OCP mutants in (a) the unquenched state, (b) the quenched state, and (c) the state after recovering from quenching. A compartmental model was constructed to describe excitation-energy transfer and trapping in *Synechocystis* using target analysis. From the target analysis, it was concluded where qE_{cya} takes place and what the (molecular) rate of quenching is. This also allowed us to draw conclusions about the mechanism of quenching and to calculate which percentage of the PB excitations reach PSI and PSII in the presence of qE_{cya}.

MATERIALS AND METHODS

Strains and Growth Conditions. The construction of the mutants without OCP protein (Δ OCP) and with overexpressed OCP protein (OverOCP) was described before (for details see refs 9, 10).

WT and mutant cells were grown photoautotrophically in a modified BG11 medium³¹ containing also 10 mM NaHCO₃ and twice the concentration of sodium nitrate. Cells were shaken in a rotary shaker (45 rpm) at 30 °C and illuminated by white lamps at 40 $\mu\text{mol} \cdot \text{m}^{-2} \cdot \text{s}^{-1}$. Mutants were grown in the presence of antibiotics (spectinomycin 25 $\mu\text{g} \cdot \text{mL}^{-1}$, streptomycin 10 $\mu\text{g} \cdot \text{mL}^{-1}$). All cells were grown in 250-mL flasks with a growing volume of 60 mL, and maintained in the logarithmic growth phase with optical densities at 800 nm (OD₈₀₀) between 0.6 and 0.8 (scattering) by refreshing the medium every 2 to 3 days.

To improve the signal-to-noise ratio of the time-resolved fluorescence measurements, cell suspensions were concentrated 3–5 times. The final suspensions were dark-adapted for 5 min before performing the fluorescence measurements.

Fluorescence Measurements. *1. Steady-State Fluorescence.* Steady-state fluorescence spectra were recorded with a Jobin Yvon Fluorolog FL3-22 spectrofluorimeter and corrected for wavelength-dependent sensitivity of the detection and fluctuations in lamp output. The excitation wavelength was 590 nm; a bandwidth of 5 nm was used for excitation and emission. Fluorescence emission spectra were recorded using a step size of 0.5 nm. Cell suspensions were diluted to a final Chl concentration of 1.0 $\mu\text{g} \cdot \text{mL}^{-1}$ and measured in a cuvette with a

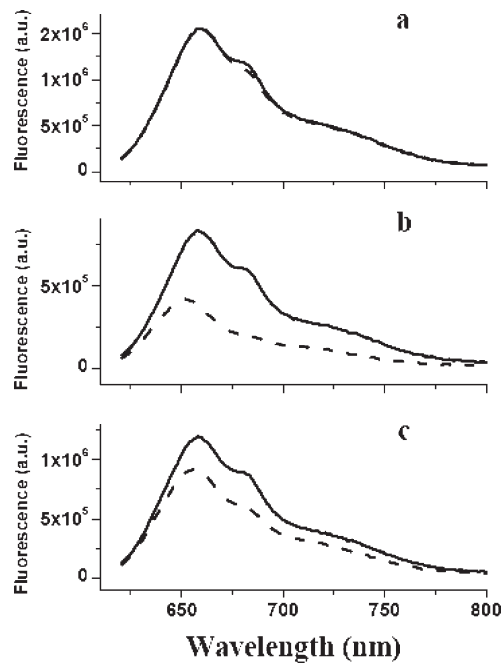


Figure 2. Room-temperature fluorescence spectra upon 590 nm excitation of cells ($1 \mu\text{g Chl/mL}$) before (solid lines) and after (dashed lines) blue-green light illumination ($220 \mu\text{E} \cdot \text{m}^{-2} \cdot \text{s}^{-1}$), (a) ΔOCP , (b) OverOCP, (c) WT.

3-mm light path to avoid significant self-absorption. Cells were quenched by illuminating with 500 nm light at $\sim 220 \mu\text{E} \cdot \text{m}^{-2} \cdot \text{s}^{-1}$ for 10 min at 20 °C and emission spectra were recorded immediately after quenching.

2. Time-Resolved Fluorescence. Time-resolved fluorescence spectra were recorded with a subpicosecond streak-camera system combined with a grating (50 grooves/mm, blaze wavelength 600 nm) with the central wavelength set at 700 nm, having a spectral width of 260 nm (for details see ref 32). Excitation light was vertically polarized, the spot size diameter was typically $\sim 100 \mu\text{m}$, and the laser repetition rate was 250 kHz. The detector polarizer was set at magic angle orientation. Great care was taken to minimize the path length (typical $\sim 100 \mu\text{m}$) to allow measurements on high-concentration samples ($\text{OD}_{680} > 3$) without significant self-absorption. Two excitation wavelengths were used: 590 and 400 nm. To avoid photodamage and to induce qE_{cya} in the entire cuvette (see below), the sample was stirred with a magnetic stirring bar (rate ~ 10 Hz) and the laser power at 590 nm was adjusted to $15 \pm 3 \mu\text{W}$. At 400 nm, the power was adjusted to $\sim 30 \pm 3 \mu\text{W}$. Images of 800 ps and 2 ns time windows were obtained for each sample and corrected for background and photocathode shading, and then sliced up into traces of 4 nm width.

For both excitation wavelengths, the instrument response function (IRF) was described with a double Gaussian, consisting of a Gaussian of ~ 9 ps fwhm (90% of IRF area) on top of a Gaussian of 100 ps fwhm (10% of IRF area).

For measuring time-resolved fluorescence of cells during quenching, an actinic white light source was used in combination with a 500 nm broad band filter (K50) giving an intensity of $\sim 350 \mu\text{E} \cdot \text{m}^{-2} \cdot \text{s}^{-1}$. The volume used for fluorescence excitation/detection was spatially well separated from the actinic light beam (a cylinder of ~ 5 mm diameter \times 1 cm length); the entire volume of the sample was 4 mL. One measurement was performed as follows: First, after 5 min of dark adaptation of the cells, fluorescence streak images were recorded for unquenched cells. Then, cells were quenched by actinic illumination at 20 °C for 1 h (to obtain the maximal quenching possible at the light

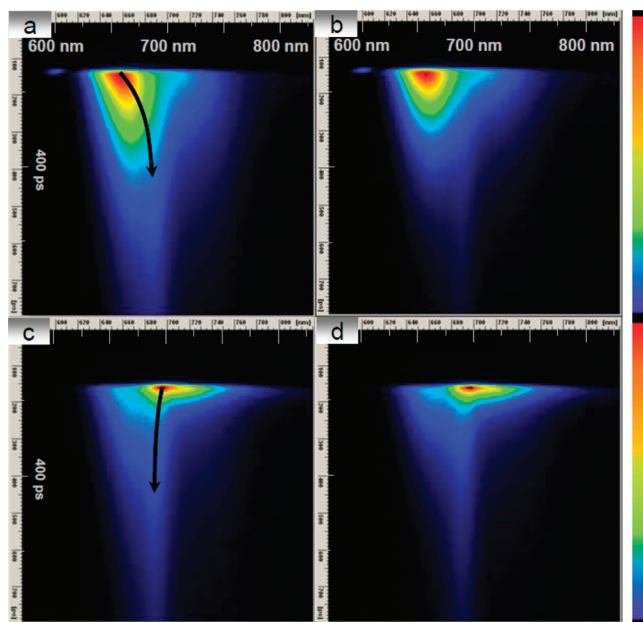


Figure 3. Streak-camera images of unquenched (a and c) and quenched (b and d) OverOCP cells. These images represent the fluorescence intensity (using a linear color gradient) as a function of time (vertical axis) and wavelength (horizontal axis); every vertical line represents a time trace of fluorescence at the corresponding wavelength, while every horizontal line reflects a fluorescence emission spectrum after a certain delay time. In panels a and b, C-Phycocyanin was selectively excited at 590 nm, and in panels c and d, Chls were selectively excited at 400 nm; all time-resolved fluorescence measurements represented in this work were repeated at least three times with cells grown on different days.

intensity used) while stirring; during subsequent measurements on quenched cells, the actinic illumination was kept on to maintain the quenched state. Finally, streak images were recorded after allowing the cells to fully recover from qE_{cya} for 1 h in the dark. At 20 °C, fluorescence recovery is slower than at 32 °C, and for the overOCP strain, it can take almost 1 h. ΔOCP , being the perfect control sample because it does not show qE_{cya} , was measured in exactly the same way as WT and Over OCP cells. A high signal-to-noise ratio was achieved by averaging 100 single images, each obtained after analog integration of 10 exposures of 1.112 s. Measurements were performed at room temperature (about 20 °C) and lasted 3 h for each sample.

3. Data Analysis. Data obtained with the streak-camera setup were first globally analyzed with the R package TIMP (for details see refs 33, 34). The methodology of global analysis is described in van Stokkum et al.³⁵ with global analysis, the data were fitted as a sum of exponential decays convolved with an IRF and the amplitudes of each decay component as a function of wavelength are called decay-associated spectra (DAS). Subsequently, ‘target analysis’ was performed as described in the Supporting Information.

RESULTS

1. Steady-State Fluorescence. Steady-state fluorescence spectra of unquenched cells of WT, OverOCP, and ΔOCP were recorded upon 590 nm excitation (Figure 2). The spectra are very similar for all unquenched cells, showing two main peaks at 660 and 680 nm. The 660 nm maximum originates from APC_{660} and the one at 680 nm from APC_{680} and/or Chl. Figure 2 also shows the spectra after 10 min of illumination with $220 \mu\text{E} \cdot \text{m}^{-2} \cdot \text{s}^{-1}$ blue-green light. For WT cells, this causes $\sim 20\%$

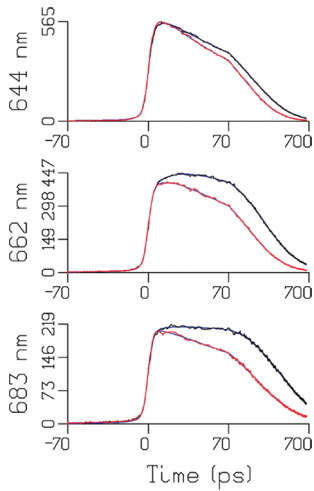


Figure 4. Emission traces at 644, 662, and 683 nm of unquenched (black) and quenched (red) OverOCP upon 590 nm excitation. Note that the time axis is linear until 70 ps, and logarithmic thereafter. Blue lines indicate the global analysis fit with five lifetimes.

fluorescence quenching, while for OverOCP, more than 50% quenching occurs. As expected, no quenching is observed for Δ OCP cells.

2. Time-Resolved Fluorescence. To determine the quenching kinetics, time-resolved fluorescence of mutant and WT cells was measured with a picosecond streak-camera system. The cells were studied in three different states: before illumination (unquenched), after illumination with strong quenching-inducing light (quenched) (illumination is continued during the measurement), and 1 h after switching off the quenching light (recovered). Either 590 nm laser pulses were used, exciting mainly C-PC (Figure 3a,b), or 400 nm pulses, exciting mainly Chls in PSI and PSII (Figure 3c,d). Figure 3a shows that the spectrum is shifting to longer wavelengths in time (red-shifting) after 590 nm excitation, which is due to downhill excitation energy transfer (EET). In contrast, Figure 3c shows that after 400 nm excitation the spectrum is slightly blue-shifting (indicated by the black arrow). The blue-shift is due to the fact that long-wavelength PSI fluorescence is shorter-lived than PSII fluorescence that contributes more at shorter wavelengths. A comparison of panels a and b in Figure 3 clearly shows that the fluorescence of unquenched OverOCP (Figure 3a) is longer-lived than that of quenched OverOCP (Figure 3b). The WT cells also show faster decay of the excited state after induction of qE_{cya} albeit less pronounced. The quenching appears to be completely reversible, meaning that the fluorescence streak images of cells that are recovered from qE_{cya} are virtually identical to the ones before qE_{cya} . As expected, no significant changes are observed for the Δ OCP cells. Upon 400 nm excitation, the effects of qE_{cya} are far less noticeable for all cell types and only a minor decrease in intensity can be observed on the short-wavelength side for WT and OverOCP cells, where PBs dominate the fluorescence.

3. Modeling Results. To get quantitative information from these images, both global analysis and target analysis were performed. Global analysis provides a minimal mathematical description of the data revealing the wavelength dependence of EET and excitation trapping. On the basis of this kinetic information, combined with a priori knowledge of the photosynthetic system, target analysis was used to construct a specific

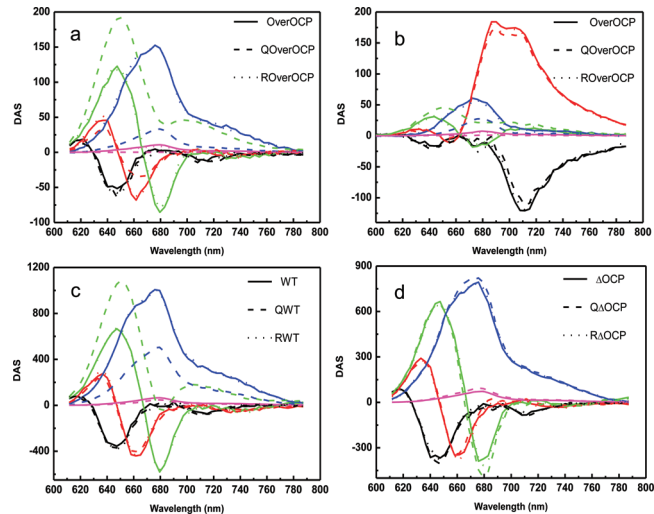


Figure 5. DAS of intact cells of OverOCP (a and b), WT (c), and Δ OCP (d), after 590 nm (a,c,d) or 400 nm excitation (b). Spectra correspond to ‘unquenched’ (solid), ‘quenched’ (dashed), labeled with Q or ‘recovered’ cells (dotted), labeled with R.

Table 1. Lifetimes of DAS^a

| Lifetimes (ps) | λ_{ex} | tau 1 | tau 2 | tau 3 | tau 4 | tau 5 |
|--|----------------|-------|-------|-------|-------|---------|
| OverOCP/ROverOCP | 590 nm | 8 | 36 | 128 | 204 | >500 ps |
| QOverOCP | 590 nm | 8 | 26 | 105 | 301 | >500 ps |
| OverOCP/ROverOCP | 400 nm | 6 | 22 | 134 | 232 | >500 ps |
| QOverOCP | 400 nm | 6 | 23 | 120 | 367 | >500 ps |
| WT/RWT | 590 nm | 9 | 39 | 122 | 195 | >500 ps |
| QWT | 590 nm | 8 | 36 | 116 | 239 | >500 ps |
| Δ OCP/Q Δ OCP/R Δ OCP | 590 nm | 8 | 38 | 121 | 205 | >500 ps |

^a Lifetimes estimated from global analysis of the fluorescence data obtained for the various cells in different states. The colors of the lifetimes correspond to the colors of the DAS in Figure 5. And the samples were named the same as in Figure 5.

compartmental model with corresponding rate constants to obtain a realistic description of the system. By exploring the model that fits best to the data, kinetic constants for the various processes (energy transfer, trapping and quenching) could be determined.

3.1. Global Analysis. 3.1.1. OverOCP. Typical unquenched (black) and quenched (red) traces for excitation at 590 nm are depicted in Figure 4 and quenching appears to be particularly well visible at 662 and 683 nm.

Global analysis of 50 emission traces of OverOCP cells reproducibly required five lifetimes. The results are shown in Figure 5a and corresponding lifetimes are given in Table 1. Induction of qE_{cya} by strong blue-green light leads to marked changes of several DAS. After switching off the blue-green light, quenching effects disappeared completely in approximately 1 h at 20 °C, demonstrating the reversibility of qE_{cya} . After cells had “recovered” from qE_{cya} , the DAS were identical to those before qE_{cya} .

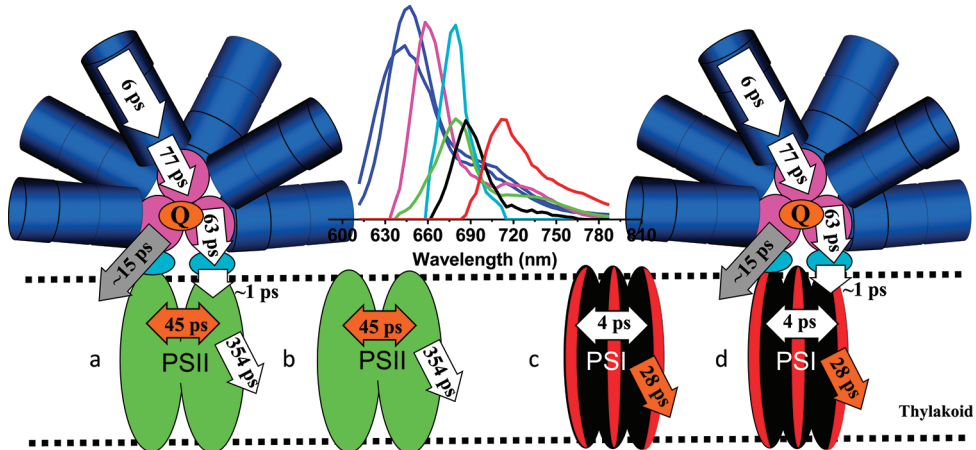


Figure 6. Schematic model showing the downhill energy transfer and trapping processes in *Synechocystis* with characteristic transfer times (a transfer time is defined as 1/transfer rate). SAS (fitting results) are shown in colors that refer to the protein complexes holding the corresponding pigments. Inverse rates of uphill energy transfer are omitted for clarity but can be found in the Supporting Information (Figure SI.2).

The black DAS in Figure 5 reflect excitation equilibration (predominantly downhill EET) in C-PC with a time constant of 8 ps, displaying a positive/negative signature, characteristic for energy transfer. The acceptor states have a higher dipolar strength than the donor states (see, e.g., ref 36) leading to a predominantly negative DAS. These DAS and their corresponding lifetimes remain unaltered upon qE_{cya} induction, showing that the corresponding transfer process is not influenced by quenching.

The red DAS with ~ 30 ps lifetime to a large extent reflect downhill EET from C-PC to APC_{660} . They are only slightly influenced by quenching because the changes in lifetime and DAS are rather small, especially when compared to the changes observed for the slower components.

The green DAS for unquenched and recovered cells with a lifetime of 130 ps reflect to a large extent EET from APC_{660} to $APC_{680} + \text{Chls}$. Like the ~ 30 ps component, they have the characteristic conservative shape with positive amplitude at short wavelengths and negative amplitude at longer wavelengths, meaning that excited-state population disappears from pigments fluorescing somewhat above 650 nm to pigments with a fluorescence maximum somewhat below 680 nm. This component is strongly influenced by the quenching; the lifetime decreases and the shape changes drastically. It loses its characteristic conservative transfer character, indicating that excitations on APC_{660} are quenched, and this leads to a shortening of the APC_{660} excited-state lifetime and a decrease in energy transfer. From these DAS it is not directly clear which percentage of the APC pigments is quenched and what the quenching rate is. These issues will be addressed below using the target analysis approach.

The dark blue DAS with 200–300 ps lifetime reflect excitation trapping by the RCs (charge separation). The DAS represents an equilibrated excitation distribution over C-PC, APC_{660} , APC_{680} , and Chls. Upon induction of qE_{cya} , the intensity of this component decreases drastically, due to the fact that many excitations are already quenched on APC_{660} before they can reach APC_{680} and Chls.

The cyan DAS with lifetimes above 500 ps have very small amplitudes. The lifetime is not well determined using the 800 ps time window; it can be varied from 600 ps to a few nanoseconds in the fit without influencing shape and position of the DAS. In data sets obtained with a 2 ns time window, the corresponding

lifetime was determined to be ~ 700 ps. These DAS probably reflect competition between secondary charge separation and charge recombination (see, e.g., ref 37), which explains why its amplitude decreases upon quenching.

Global analysis of the results that are obtained upon 400 nm excitation leads to the DAS that are shown in Figure 5b. Using 400 nm pulses, excitations are mainly created in PSI and PSII and only 10% is created in PB,³⁰ leading to the fluorescence on the short-wavelength side of the image. The latter excitations give rise to the same DAS and quenching kinetics as the excitations created by 590 nm laser pulses (see Figure 5b). The dominating component of 22 ps (red DAS in Figure 5b) represents emission from Chls in PSI,^{30,38,39} which appears to be hardly quenched.

3.1.2. WT and ΔOCP . The DAS that are obtained for unquenched WT and ΔOCP cells (see Figure 5, panels c and d, respectively) are virtually identical to those obtained for unquenched OverOCP cells. This shows that the organization of the photosynthetic system is identical in all cases, but also it testifies to the high reproducibility of both measurement and analysis. The fluorescence kinetics of ΔOCP cells are hardly affected by illumination with strong blue-green light, but for WT cells, similar changes are induced as for OverOCP cells, although the effects of qE_{cya} are less pronounced. EET within the C-PC rods and from C-PC to APC are nearly unaffected in WT cells since the 2 DAS with the shortest lifetimes remain nearly the same. The third DAS, which is conservative in the absence of quenching, becomes strongly nonconservative, again reflecting quenching of APC_{660} . However, the strong dip around 680 nm indicates that still a substantial amount of EET toward APC_{680} and Chls takes place, also explaining why the fourth and fifth DAS decrease less in intensity for WT than for OverOCP. It is not immediately clear whether a larger fraction of PB remains unquenched as compared to OverOCP or whether the quenching rate is smaller. This issue will be addressed below.

In summary, global analysis of the presented time-resolved fluorescence data indicates that APC_{660} is quenched directly in vivo. However, it is not clear which fraction of the PB is quenched and what the rate of quenching is. To resolve these issues, target analysis was performed.

3.2. Target Analysis. It is known that PBs can transfer energy to both PSI and PSII.^{27,28} Thus, a good model requires the presence

of PB coupled to PSII (PB–PSII) and to PSI (PB–PSI). To obtain acceptable fitting results, it was discovered that the amount of excitations being transferred from PB to PSII and PSI had to be rather similar (for more details see Supporting Information). PB was allowed to be quenched or unquenched and the fraction of quenched PB was included as a free fitting parameter. Quenched PB–PSII and PB–PSI are shown in Figure 6, whereas the unquenched versions are omitted from the figure for clarity. It has been reported that also uncoupled PB should be present,²⁹ but since the corresponding lifetime of 1.2–1.5 ns was not observed in our study, their amount was considered to be insignificant.

A correct description of the 400 nm data requires the presence of two additional pigment–protein structures: PSII and PSI without any coupled PBs (schematic structures of PSII and PSI are also included in Figure 6). Details about the fitting and input parameters are shown in the Supporting Information (Figure SI.2 and Table SI.1). The SAS resulting from the analysis are assigned based on the positions of their maxima: the two blue SAS correspond to short- and long wavelength forms of C-PC (here named PC-S and PC-L, respectively); the magenta SAS with maximum around 660 nm corresponds to APC₆₆₀; the cyan SAS and the green SAS with maximum around 680 nm correspond to APC₆₈₀ and Chls in PSII, respectively. The black and red SAS originate from bulk Chls (688 nm) and red Chls (712 nm) in PSI, respectively, which is in perfect agreement with previous reports on isolated PSI.^{38,40} As pointed out in the Supporting Information, also energy transfer rates are in agreement with reports on PSI, PSII, and PBs and subcomplexes thereof and the same is true for the fluorescence spectra (SAS) of the various pigments.

To determine in which of the different pigment pools the blue-green light-induced quenching takes place, one additional decay rate constant k_Q (reflecting the quenching) was added in turn to the various compartments and the data for the quenched cells was fitted keeping all other rate constants the same as for the unquenched cells. The results were unequivocal: only quenching of the APC₆₆₀ compartment leads to a satisfactory fit of the data and the corresponding quenching rate is $66 \pm 15 \text{ ns}^{-1}$ for OverOCP. Putting the quencher in another compartment resulted in fits of lesser quality or led to unrealistic SAS. Another important finding was that not all PBs are quenched. For OverOCP, the percentage of quenched PBs was found to be ~72%.

With the same model, the data on WT cells could be fitted equally well, the main difference being that only ~29% of all PBs appeared to be quenched whereas the quenching rate was 54 ns^{-1} rather similar to that of OverOCP. This explains why, in steady-state spectra, the quenching ratio in WT cells is only about one-third of that in OverOCP cells.

For the ΔOCP mutant, the same target model was successfully applied (results not shown) for all three measuring states (before, during, and after applying high intensity blue-green light) and the results are similar to those for unquenched WT and OverOCP cells.

■ DISCUSSION

1. The Location, Rate, and Efficiency of qE_{cya} . It was demonstrated before with steady-state fluorescence measurements on various *Synechocystis* mutants and in vitro reconstitution experiments that quenching takes place in the APC core of the PB^{9,11,13,15} and our current data confirm this. However, due

to fast EET from APC₆₆₀ to APC₆₈₀/Chls it could not be determined before whether APC₆₆₀ or APC₆₈₀²⁰ was quenched and also the quenching rate remained unknown. It is now revealed that quenching takes place at the level of APC₆₆₀ and not APC₆₈₀. The rate of quenching of the APC₆₆₀ pool turns out to be $66 \pm 15 \text{ ns}^{-1}$ (which is equivalent to $(16 \pm 4 \text{ ps})^{-1}$). This is extremely fast and leads to efficient quenching. From the parameters obtained with the target analysis, it can be concluded that in the presence of qE_{cya} , 80% of the excitations that are harvested by a quenched PB are dissipated as heat before reaching PSII and PSI (see Supporting Information). Our results indicate that both PSI and PSII are protected. However, not all PBs are in the quenched state. The number of quenched PBs depends on the ratio OCP^r to PB¹¹. In WT cells, there is only 1 OCP per 2–3 PB. Moreover, not all OCP is expected to be in the OCP^r state in the used light conditions, although the exact amount of activated OCP is unknown. Indeed, we found that only 29% of the PBs were quenched for WT cells. For OverOCP cells, the concentration of OCP is about 7- to 8-fold higher than in WT, meaning more than 2–3 OCP per PB²¹. Consistently, the number of quenched PBs is substantially higher, namely, 72%.

2. The Mechanism of qE_{cya} at the Molecular Level. Our present study has disclosed that one of the APC₆₆₀ pigments is directly quenched (from now on we call this quenched pigment APC^Q₆₆₀). The overall quenching rate of the APC₆₆₀ pool appears to be $66 \pm 15 \text{ ns}^{-1}$ or $(16 \pm 4 \text{ ps})^{-1}$. Since there are approximately 66 APC₆₆₀ pigments present in one PB core, the molecular quenching rate of APC^Q₆₆₀ is at most $(0.24 \pm 0.06 \text{ ps})^{-1}$, corresponding to 16/66 ps in case EET within the APC₆₆₀ pool is infinitely fast. In the case of infinitely fast EET, the probability that the excitation is on the quenched pigment is 1/66 which slows down the molecular quenching rate by a factor of 66. Slower EET requires an even faster quenching rate (see, e.g., ref 37).

It has been hypothesized that the C-terminal OCP domain, by interacting with the center of an APC trimer, may bring the carotenoid into proximity of the APC chromophores, whereas light-induced carotenoid changes could then regulate the interaction between the carotenoid and the APC chromophores (either $\alpha 84$ or $\beta 84$).¹⁰ Support for this hypothesis comes from the fact that the C-terminal domain of OCP is structurally similar to the 7.8 kDa core linker protein that is bound within the central aperture of the APC trimer and directly interacts with the $\beta 84$ chromophores of two APC subunits. The present findings indeed confirm the direct quenching of one of the APC chromophores and the ultrafast quenching rate suggests extremely strong coupling between one of the APC chromophores and the OCP carotenoid hECN.

One could envision several carotenoid-induced quenching mechanisms occurring based on the analogy of chlorophyll quenching by carotenoids: (1) excitonic coupling^{41–43} between APC^Q₆₆₀ and hECN, (2) EET from APC^Q₆₆₀ to the S₁ state of hECN,^{44,45} (3) electron transfer from hECN to APC^Q₆₆₀.⁴⁶ The same three mechanisms were also recently identified for tetrapyrrole singlet excited state quenching by carotenoids in artificial systems.⁴⁷

The fact that the quenching rate is faster than $(1 \text{ ps})^{-1}$ rules out the first mechanism because the excited-state decay rate would be a weighted average of the excited-state decay rate of APC₆₆₀ and of hECN in the absence of interaction.⁴³ Because the excited-state lifetime of hECN is above 1 ps and that of APC₆₆₀ even above 1 ns, it is impossible to obtain an average lifetime which is 0.24 ps or even shorter.

It is more difficult to estimate whether EET from APC^Q₆₆₀ to the S₁ state of hECN might happen with a rate of (0.24 ± 0.06 ps)⁻¹. Up to now, rates of EET from the lowest excited state of (B)Chls/bilins to the carotenoid S₁ state have not been measured for pigment–protein complexes. However, various studies have reported rates for EET from the carotenoid S₁ state to the lowest Q_y states of (bacterio)chlorophylls. Both types of rates are expected to be similar because the electronic coupling mechanism is the same, while mainly the relative ordering of the energy levels of both molecules differs in both cases. Carotenoid-to-BChl *a* energy transfer times involving the S₁ state were reported to be of the order of several picoseconds for light-harvesting complexes from purple bacteria.^{48–52} This is an order of magnitude slower than the obtained quenching rate in the present study. A larger spread in transfer times was reported for Chl *a* containing light-harvesting complexes LHCII and CP29.^{53–56} Whereas Croce et al. hardly observed any transfer from the S₁ state in LHCII from plants,⁵³ a time constant of ~1 ps was reported by Gradinaru et al.,⁵⁴ whereas Walla et al. found several transfer times, ranging from ~200 fs to over 7 ps.⁵⁵ For CP29, Croce et al. reported different transfer times for the different carotenoids in CP29,⁵⁶ the fastest being 700 fs, whereas Gradinaru et al. found a time of around 1 ps.⁵⁴

It is important to note that a transient absorption study was performed on a model system made up of a zinc phtalocyanine (*Pc*) molecule (similar to Chl) covalently linked to carotenoids with 9, 10, or 11 conjugated carbon–carbon double bonds.⁵⁷ By increasing the number of double bonds, the S₁ energy level becomes lower than the lowest excited singlet energy level of the *Pc* molecule. EET could be observed from *Pc* to the Car in the case of 10 and 11 conjugated double bonds and the transfer rates varied from (56 ps)⁻¹ to (17 ps)⁻¹, depending on solvent polarity and conjugation length, that is, far slower than the observed quenching rate in the present study. We conclude that most of the experimentally obtained transfer rates are slower or even far slower than the lower limit for the quenching rate of (0.24 ± 0.06 ps)⁻¹ but we cannot entirely exclude that EET from APC^Q₆₆₀ to the S₁ state of hECN might be responsible for qE_{cya}.

Finally, it has been reported that in plants nonphotochemical quenching can occur via charge transfer within a closely coupled excited pair of a Chl *a* molecule and a zeaxanthin carotenoid molecule with a time constant between 0.1 and 1.0 ps, leading to fluorescence quenching of Chl.^{46,58} The rate of ($\sim 0.24 \pm 0.06$ ps)⁻¹ for APC quenching in cyanobacteria falls nicely within this interval. Therefore, based on the available data, it appears most likely that charge transfer from the red form of hECN in OCP to APC^Q₆₆₀ in the PB core is responsible for the blue-green light-induced nonphotochemical quenching in cyanobacteria.

■ ASSOCIATED CONTENT

S Supporting Information. Scheme of the model, inputs and fitting parameters of target analysis and fitting quality. This material is available free of charge via the Internet at <http://pubs.acs.org>.

■ AUTHOR INFORMATION

Corresponding Author

Herbert.vanAmerongen@wur.nl

■ ACKNOWLEDGMENT

We thank Dr. S. Laptenok (Ecole Polytechnique, 91128 Palaiseau, France) and J. Snellenburg (VU Amsterdam University) for help with the use of the TIMP package, C. Wolfs (Wageningen UR) for help in growing the cells and Arie van Hoek (Wageningen UR) for technical support. This work was supported by a fellowship to L.T. from the Graduate School Experimental Plant Sciences (EPS), Wageningen, The Netherlands, by the Dutch Ministry of ELI through the BioSolar Cells Project and by the European community via the HARVEST project.

■ REFERENCES

- (1) Aro, E.-M.; Virgin, I.; Andersson, B. *Biochim. Biophys. Acta, Bioenerg.* **1993**, *1143*, 113–134.
- (2) Tyystjärvi, E. *Coord. Chem. Rev.* **2008**, *252*, 361–376.
- (3) Vass, I. *Physiol. Plant.* **2011**, *142*, 6–16.
- (4) Horton, P.; Ruban, A. V.; Walters, R. G. *Annu. Rev. Plant Phys.* **1996**, *47*, 655–684.
- (5) Niyogi, K. K. *Annu. Rev. Plant Phys.* **1999**, *50*, 333–359.
- (6) Kirilovsky, D. *Photosynth. Res.* **2007**, *93*, 7–16.
- (7) El Bissati, K.; Delphin, E.; Murata, N.; Etienne, A. L.; Kirilovsky, D. *Biochim. Biophys. Acta, Bioenerg.* **2000**, *1457*, 229–242.
- (8) Rakhimberdieva, M. G.; Stadnichuk, I. N.; Elanskaya, T. V.; Karapetyan, N. V. *FEBS Lett.* **2004**, *574*, 85–88.
- (9) Wilson, A.; Ajlani, G.; Verbavatz, J. M.; Vass, I.; Kerfeld, C. A.; Kirilovsky, D. *Plant Cell* **2006**, *18*, 992–1007.
- (10) Wilson, A.; Punginelli, C.; Gall, A.; Bonetti, C.; Alexandre, M.; Routaboul, J. M.; Kerfeld, C. A.; van Grondelle, R.; Robert, B.; Kennis, J. T. M.; Kirilovsky, D. *Proc. Natl. Acad. Sci. U.S.A.* **2008**, *105*, 12075–12080.
- (11) Gwizdala, M.; Wilson, A.; Kirilovsky, D. *Plant Cell* **2011**, *23*, 2631–2643.
- (12) Boulay, C.; Wilson, A.; D’Haene, S.; Kirilovsky, D. *Proc. Natl. Acad. Sci. U.S.A.* **2010**, *107*, 11620–11625.
- (13) Scott, M.; McCollum, C.; Vasil’ev, S.; Crozier, C.; Espie, G. S.; Krol, M.; Huner, N. P. A.; Bruce, D. *Biochemistry* **2006**, *45*, 8952–8958.
- (14) Rakhimberdieva, M. G.; Bolychevtsva, Y. V.; Elanskaya, I. V.; Karapetyan, N. V. *FEBS Lett.* **2007**, *581*, 2429–2433.
- (15) Rakhimberdieva, M. G.; Vavilin, D. V.; Vermaas, W. F. J.; Elanskaya, I. V.; Karapetyan, N. V. *Biochim. Biophys. Acta, Bioenerg.* **2007**, *1767*, 757–765.
- (16) Wilson, A.; Boulay, C.; Wilde, A.; Kerfeld, C. A.; Kirilovsky, D. *Plant Cell* **2007**, *19*, 656–672.
- (17) Boulay, C.; Abasova, L.; Six, C.; Vass, I.; Kirilovsky, D. *Biochim. Biophys. Acta, Bioenerg.* **2008**, *1777*, 1344–1354.
- (18) Rakhimberdieva, M. G.; Elanskaya, I. V.; Vermaas, W. F. J.; Karapetyan, N. V. *Biochim. Biophys. Acta, Bioenerg.* **2010**, *1797*, 241–249.
- (19) Wilson, A.; Kinney, J. N.; Zwart, P. H.; Punginelli, C.; D’Haene, S.; Perreau, F.; Klein, M. G.; Kirilovsky, D.; Kerfeld, C. A. *J. Biol. Chem.* **2010**, *285*, 18364–18375.
- (20) Rakhimberdieva, M. G.; Kuzminov, F. I.; Elanskaya, I. V.; Karapetyan, N. V. *FEBS Lett.* **2011**, *585*, 585–589.
- (21) Kirilovsky, D.; Kerfeld, C. A. *Biochim. Biophys. Acta* **2011**, DOI:10.1016/j.bbabiobio.2011.04.013.
- (22) Glazer, A. N. *Biochim. Biophys. Acta* **1984**, *768*, 29–51.
- (23) Grossman, A. R.; Schaefer, M. R.; Chiang, G. G.; Collier, J. L. *Microbiol. Rev.* **1993**, *57*, 725–749.
- (24) MacColl, R. *J. Struct. Biol.* **1998**, *124*, 311–334.
- (25) Adir, N. *Photosynth. Res.* **2005**, *85*, 15–32.
- (26) Arteni, A. A.; Ajlani, G.; Boekema, E. J. *Biochim. Biophys. Acta, Bioenerg.* **2009**, *1787*, 272–279.
- (27) Ashby, M. K.; Mullineaux, C. W. *Photosynth. Res.* **1999**, *61*, 169–179.
- (28) Dong, C.; Tang, A.; Zhao, J.; Mullineaux, C. W.; Shen, G.; Bryant, D. A. *Biochim. Biophys. Acta, Bioenerg.* **2009**, *1787*, 1122–1128.

- (29) Bittersmann, E.; Vermaas, W. *Biochim. Biophys. Acta* **1991**, *1098*, 105–116.
- (30) Krumova, S. B.; Laptenok, S. P.; Borst, J. W.; Ughy, B.; Gombos, Z.; Ajlani, G.; van Amerongen, H. *Biophys. J.* **2010**, *99*, 2006–2015.
- (31) Rippka, R.; Deruelles, J.; Waterbury, J. B.; Herdman, M.; Stanier, R. Y. *J. Gen. Microbiol.* **1979**, *111*, 1–61.
- (32) Stokkum, I. H. M.; Oort, B.; Mourik, F.; Gobets, B.; Amerongen, H. In *Biophysical Techniques in Photosynthesis*; Aartsma, T. J., Matysik, J., Eds.; Springer: Netherlands: 2008; Vol. 26, pp 223–240.
- (33) Laptenok, S. P.; Borst, J. W.; Mullen, K. M.; van Stokkum, I. H. M.; Visser, A. J. W. G.; van Amerongen, H. *Phys. Chem. Chem. Phys.* **2010**, *12*, 7593–7602.
- (34) Mullen, K. M.; van Stokkum, I. H. M. *J. Stat. Software* **2007**, *18*, 1–46.
- (35) van Stokkum, I. H. M.; Larsen, D. S.; van Grondelle, R. *Biochim. Biophys. Acta, Bioenerg.* **2004**, *1657*, 82–104.
- (36) van Amerongen, H.; Valkunas, L.; van Grondelle, R. *Photosynthetic Excitons*; World Scientific Publishing Co.Pte.Ltd.: River Edge, NJ, 2000.
- (37) Broess, K.; Trinkunas, G.; van Hoek, A.; Croce, R.; van Amerongen, H. *Biochim. Biophys. Acta, Bioenerg.* **2008**, *1777*, 404–409.
- (38) Gobets, B.; van Grondelle, R. *Biochim. Biophys. Acta, Bioenerg.* **2001**, *1507*, 80–99.
- (39) van Oort, B.; Amunts, A.; Borst, J. W.; van Hoek, A.; Nelson, N.; van Amerongen, H.; Croce, R. *Biophys. J.* **2008**, *95*, 5851–5861.
- (40) Gobets, B.; van Stokkum, I. H. M.; van Mourik, F.; Dekker, J. P.; van Grondelle, R. *Biophys. J.* **2003**, *85*, 3883–3898.
- (41) Lampoura, S. S.; Barzda, V.; Owen, G. M.; Hoff, A. J.; van Amerongen, H. *Biochemistry* **2002**, *41*, 9139–9144.
- (42) Bode, S.; Quentmeier, C. C.; Liao, P. N.; Hafi, N.; Barros, T.; Wilk, L.; Bittner, F.; Walla, P. J. *Proc. Natl. Acad. Sci. U.S.A.* **2009**, *106*, 12311–12316.
- (43) van Amerongen, H.; van Grondelle, R. *J. Phys. Chem. B* **2001**, *105*, 604–617.
- (44) Ruban, A. V.; Berera, R.; Illoiaia, C.; van Stokkum, I. H. M.; Kennis, J. T. M.; Pascal, A. A.; van Amerongen, H.; Robert, B.; Horton, P.; van Grondelle, R. *Nature* **2007**, *450*, 575–U22.
- (45) Young, A. J.; Phillip, D.; Ruban, A. V.; Horton, P.; Frank, H. A. *Pure Appl. Chem.* **1997**, *69*, 2125–2130.
- (46) Holt, N. E.; Zigmantas, D.; Valkunas, L.; Li, X. P.; Niyogi, K. K.; Fleming, G. R. *Science* **2005**, *307*, 433–436.
- (47) Kloz, M.; Pillai, S.; Kodis, G.; Gust, D.; Moore, T. A.; Moore, A. L.; van Grondelle, R.; Kennis, J. T. *J. Am. Chem. Soc.* **2011**, *133*, 7007–15.
- (48) Walla, P. J.; Linden, P. A.; Hsu, C. P.; Scholes, G. D.; Fleming, G. R. *Proc. Natl. Acad. Sci. U.S.A.* **2000**, *97*, 10808–13.
- (49) Zhang, J.-P.; Fujii, R.; Qian, P.; Inaba, T.; Mizoguchi, T.; Koyama, Y.; Onaka, K.; Watanabe, Y.; Nagae, H. *J. Phys. Chem. B* **2000**, *104*, 3683–3691.
- (50) Polívka, T.; Pullerits, T.; Frank, H. A.; Cogdell, R. J.; Sundström, V. *J. Phys. Chem. B* **2004**, *108*, 15398–15407.
- (51) Cong, H.; Niedzwiedzki, D. M.; Gibson, G. N.; LaFountain, A. M.; Kelsh, R. M.; Gardiner, A. T.; Cogdell, R. J.; Frank, H. A. *J. Phys. Chem. B* **2008**, *112*, 10689–703.
- (52) Polívka, T.; Frank, H. A. *Acc. Chem. Res.* **2010**, *43*, 1125–1134.
- (53) Croce, R.; Müller, M. G.; Bassi, R.; Holzwarth, A. R. *Biophys. J.* **2001**, *80*, 901–915.
- (54) Gradinaru, C. C.; van Stokkum, I. H. M.; Pascal, A. A.; van Grondelle, R.; van Amerongen, H. *J. Phys. Chem. B* **2000**, *104*, 9330–9342.
- (55) Walla, P. J.; Linden, P. A.; Ohta, K.; Fleming, G. R. *J. Phys. Chem. A* **2001**, *106*, 1909–1916.
- (56) Croce, R.; Müller, M. G.; Caffarri, S.; Bassi, R.; Holzwarth, A. R. *Biophys. J.* **2003**, *84*, 2517–2532.
- (57) Berera, R.; Herrero, C.; van Stokkum, I. H. M.; Vengris, M.; Kodis, G.; Palacios, R. E.; van Amerongen, H.; van Grondelle, R.; Gust, D.; Moore, T. A.; Moore, A. L.; Kennis, J. T. M. *Proc. Natl. Acad. Sci. U.S.A.* **2006**, *103*, 5343–5348.
- (58) Ahn, T. K.; Avenson, T. J.; Ballottari, M.; Cheng, Y. C.; Niyogi, K. K.; Bassi, R.; Fleming, G. R. *Science* **2008**, *320*, 794–797.

Site, rate and mechanism of photoprotective quenching in cyanobacteria.

Lijin Tian^a, Ivo H.M. van Stokkum^b, Rob B.M. Koehorst^a, Aniek Jongerius^a, Diana Kirilovsky^c and Herbert van Amerongen^{a,d,*}.

^a *Laboratory of Biophysics, Wageningen University, PO Box 8128,6700 ET, Wageningen, The Netherlands*

^b *Biophysics Group, Department of Physics and Astronomy, Faculty of Sciences, VU University, DeBoelelaan1081, 1081 HV Amsterdam, The Netherlands*

^c *Commissariat à l'Energie Atomique, Institut de Biologie et Technologies de Saclay and Centre National de la Recherche Scientifique, 91191 Gif sur Yvette, France*

^d *MicroSpectroscopy Centre, Wageningen University, PO Box 8128,6700 ET, Wageningen, The Netherlands*

Target analysis of NPQ in cyanobacteria *in vivo*

The target analysis takes into account the following *a priori* knowledge:

- PBs can transfer energy to both PSII and PSI (Ashby and Mullineaux 1999; Dong, Tang et al. 2009).
- Part of PSII and PSI is not coupled to PBs (Ohki, Okabe et al. 1987).
- Approximately 10% of the 590 nm excitations is absorbed by PSII and PSI, the remainder is absorbed by PC-S (Krumova, Laptenok et al. 2010).
- Approximately 10% of the 400 nm excitations is absorbed by PBs, mainly by PC-S and PC-L. The remainder is absorbed by PSII and PSI (Krumova, Laptenok et al. 2010).
- A fraction of the PBs is thought to be unquenched. For WT it is known that OCP is present in a substoichiometric amount as compared to PBs (Kirilovsky and Kerfeld 2011).
- PSII can be in an open or a closed state.
- All energy transfer is in principle reversible.

The *a priori* knowledge is partly visualized in the cartoon model depicted in Fig.SI.1.

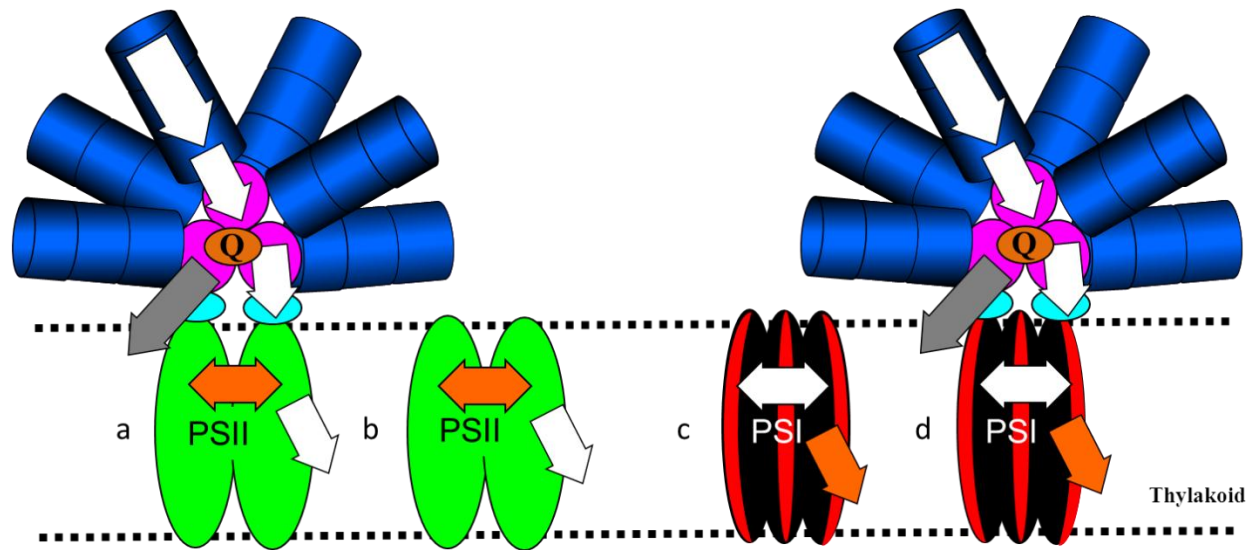


Fig.SI.1: Cartoon model of excitation energy, electron transfer and excited-state quenching in the thylakoid membrane of cyanobacteria. Arrows indicate the flow of excitation energy, charge separation (orange arrow) and excited-state quenching (grey). Q indicates that a PBS can be quenched. Two additional assemblies have been omitted for clarity: One is like the 'a' assembly but it is not quenched (NQ instead of Q) and the other is like assembly 'd' and is also not quenched.

Fig.SI.1 contains six different assemblies of pigment-protein complexes: PSI and PSII without any coupled PB, PSII and PSI coupled to PBs that can be quenched (Q), PSI and PSII coupled to PBs that cannot be quenched (NQ, not depicted in the cartoon). The 590 nm excitation light preferentially excites PB (90%), thus not providing much information on PSI and PSII kinetics. The 400 nm excitation light preferentially excites PSI and PSII (90%), thus providing the missing information. In order to describe the complete dynamics four PBs compartments are

distinguished: PC-S, PC-L, APC₆₆₀, and APC₆₈₀. It is well known that PSI can be adequately described with two compartments: bulk Chl (about 100 Chl, including RC), from which charge separation occurs and which is in equilibrium with red Chl (6 Chl) (Gobets and van Grondelle 2001; Gobets, van Stokkum et al. 2001). In the PSII core 35 Chls are present. When the PSII RC is open, charge separation is not entirely irreversible, and an equilibrium (Miloslavina, Szczepaniak et al. 2006; van der Weij-de Wit, Dekker et al. 2011) between the excited state of the system and the first radical pair state is needed to describe PSII core emission. When the PSII RC is closed, the equilibrium with the first radical pair state shifts towards the excited state. Since the exact amount of open PSII RCs is not known, PSII core emission is described with two compartments: antenna plus RC (35 Chl) in equilibrium with a non radiative (NR) compartment, where the rate constants of this equilibrium are free fitting parameters, and thus can effectively describe a mixture of open and closed RCs.

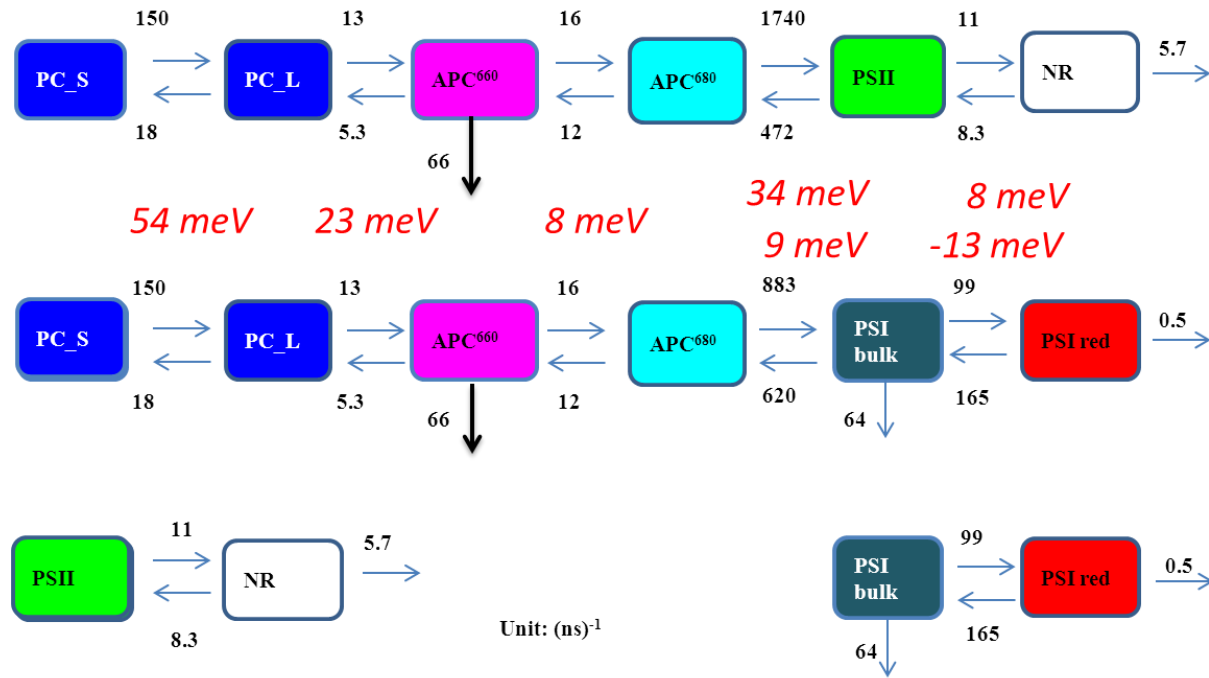


Fig.SI.2: Kinetic scheme used for target analysis of time-resolved fluorescence data of quenched and unquenched cyanobacteria *in vivo*. Rates estimated from the OverOCP data in Fig.SI.3 (further explanation, see below) are given in (ns)⁻¹. Differences in free energy between compartments were calculated from these estimated rates and are indicated in red italic.

In the target analysis 28 compartments are used as partly depicted in Fig.SI.2: PSII and PSI without any coupled PBs each require two compartments; the PBs “energy funnel” PC-S, PC-L, APC₆₆₀, APC₆₈₀ can be either quenched or unquenched, and it can be in equilibrium with PSII or PSI. This leads to 2x2+4x(4+2)=28 compartments. Fortunately, the Species Associated Spectra (SAS) of PC-S, PC-L, APC₆₆₀, APC₆₈₀, PS II, PS I bulk (PSIb), PS I red (PSIr) can be linked, and only 7 SAS need to be estimated. The nonradiative (NR) compartment has a zero SAS. Note

that the rate constants of the energy funnel PC-S, PC-L, APC₆₆₀, APC₆₈₀ are assumed to be identical for the four different cases (PB-PS II Q, PB-PS II NQ, PB-PS I Q, PB-PS I NQ), and also the rate constants of PSII or PSI are assumed to be identical for the three different cases (without any coupled PBs, Q and NQ). Several possibilities for the quenching of PBs were tested, and in Fig.SI.2 only the most important quenching rate, from APC₆₆₀ is shown. Thus in total 18 different rate constants are needed to describe one experiment. This is much more than the five lifetimes estimated from the global analysis. Therefore, four different experiments (see also Fig.SI.3) are analysed simultaneously: unquenched 590 (black), quenched 590 (red), unquenched 400 (blue), quenched 400 (green) nm excitation. This simultaneous target analysis allows to resolve all SAS (see below).

Also alternative kinetic schemes were tried. Most important was a scheme where the quenching starts from APC₆₈₀ instead of APC₆₆₀ because it is not immediately obvious from the global analysis where in the core the quenching takes place. However, this fit resulted in a huge increase in the root mean square error (rmse), and it proved to be impossible to describe the data with this scheme. This made us conclude that the quenching is not located on APC₆₈₀. Therefore we report here only on the scheme of Fig.SI.2.

Input parameters

Next to the rate constants, also the inputs (fractions of excitation) to the different PC-S, PC-L (only with 400 nm excitation), PSII, PSI bulk, PSI red compartments must be estimated. But the values of these inputs are mutually dependent. The following *a priori* knowledge/assumptions/definitions are employed:

- The relative absorption of PSII at 590 nm is given by the parameter $\varepsilon 2_{590}$ (2 for PSII) which is fixed at 1, and the absorption of PSII at 400 nm is a parameter $\varepsilon 2_{400}$ to be estimated. Likewise, parameters εc_{590} and εc_{400} (c for phycoCyanin) reflect the relative absorption of PBSs at 590 and 400 nm.
- PSI absorbs α times more than PSII. Thus $\varepsilon 1_{590}$ (1 for PSI) is α times $\varepsilon 2_{590}$, and $\varepsilon 1_{400} = \alpha \cdot \varepsilon 2_{400}$. In view of the ~106 vs. 35 Chls, α is fixed at 3.
- The red Chl compartment of PSI is represented by a fraction r , and the PS I bulk compartment by $1-r$. In view of the 6 red Chls r is fixed at 0.06.
- PC-S and PC-L have equal absorption at 400 nm, and only PC-S absorbs at 590 nm.
- A fraction $c2$ of the PBs is linked to PSII and a fraction $c1 = 1 - c2$ to PSI. It is assumed that $c1 = c2 = 0.5$. This ratio was necessary to get a reasonable PSI/II ratio and SAS with comparable amplitudes for all pigments.
- PBs can be in a quenched state (fraction q) or in an unquenched state (fraction $1-q$) and the parameter q has to be estimated.

- The input to PSII and PSI without any coupled PB at 590 nm is represented by the parameters $l2_{590}$ and $l1_{590}$ (l for loose). Since $\varepsilon2_{590} \equiv 1$, $l2_{400} = l2_{590} \cdot \varepsilon2_{400}$ and $l1_{400} = l1_{590} \cdot \varepsilon2_{400}$. 

There are 17 compartments that receive input:

- PC-S, PC-L quenched or unquenched, in equilibrium with PSII or PSI: 2x4
- PSII, PSIb, PSIr coupled to PBs quenched or unquenched, and not coupled to PBs (loose): 3x3.

Using the above assumptions and definitions the input to these 17 compartments with 400 and 590 nm excitation (totalling 34 input values) are described by only six free parameters:

Quenching fraction q , absorption parameters $\varepsilon2_{400}, \varepsilon c_{400}, \varepsilon c_{590}, l2$ and $l1$.

For example: the input to the nonquenched PSIr coupled to PBs at 400 nm is given by

$$(1-q) \cdot r \cdot \varepsilon l_{400} \cdot c1 = (1-q) \cdot r \cdot \alpha \cdot \varepsilon2_{400} \cdot c1 = (1-q) \cdot 0.06 \cdot 3 \cdot \varepsilon2_{400} \cdot 0.5$$

Spectral assumptions

As explained above, only 7 SAS need to be estimated. The following spectral assumptions have been used:

- to estimate the equilibrium between PS I bulk and PS I red: $SAS_{PSIr} = 0$ below 686 nm,
- to facilitate resolution of SAS, and to ensure nonnegativity: $SAS_{APC660} = 0$ below 634 nm,
- $SAS_{APC680} = 0$ below 661 nm and above 715 nm,
- $SAS_{PSIb} = 0$ below 665 nm and above 770 nm,
- $SAS_{PSII} = 0$ below 640 nm.

Thus the number of free spectral parameters (50 different wavelengths) was reduced from $7 \times 50 = 350$ to 259.

Other parameters

In Materials and Methods the instrument response function (IRF) was already introduced; it is described with a double Gaussian, consisting of a narrow Gaussian of 9 ps FWHM (90% of the IRF area) on top of a broader Gaussian of 100 ps FWHM (10% of the IRF area). The location of this IRF is wavelength-dependent due to the streak-camera properties, and it is well described by a parabola (van Stokkum, van Oort et al. 2008). The simultaneous analysis of four experiments requires three relative scaling parameters.

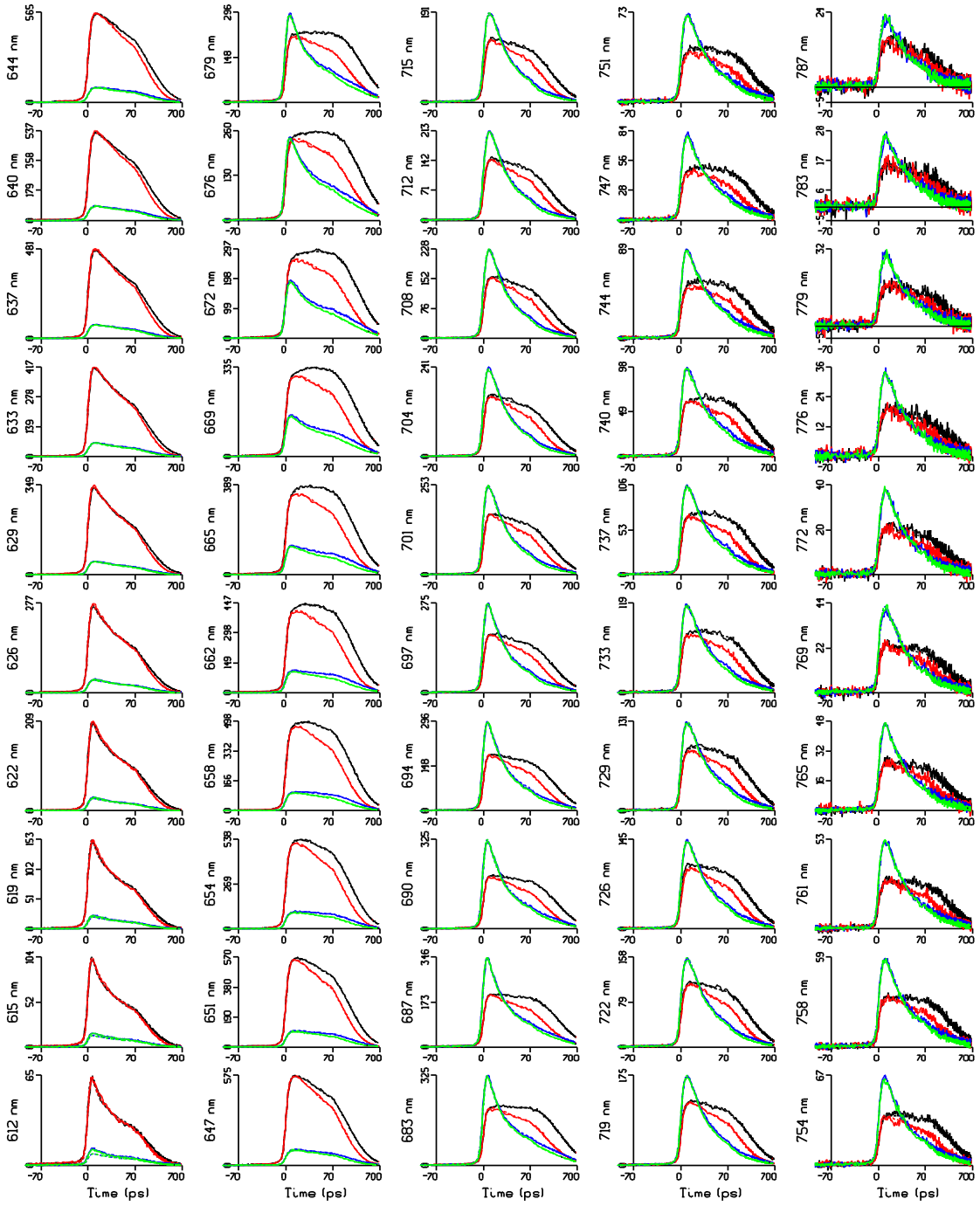


Fig.SI.3 Emission of OverOCP at 50 wavelengths, as obtained from the four streak images in Fig.2. Key: unquenched 590 (black), quenched 590 (red), unquenched 400 (blue), quenched 400 (green) nm excitation. Note that the time axis is linear until 70 ps and logarithmic thereafter. Dashed lines indicate the simultaneous target analysis fit.

Simultaneous target analysis

In the above we have explained how we can compute the concentrations of all compartments. For each of the seven emitting species (PC-S, PC-L, APC₆₆₀, APC₆₈₀, PS II, PS I bulk, and PS I red), we can add the concentrations of all compartments belonging to that species. Thus we arrive at a concentration matrix C for each excitation wavelength (400 and 590 nm) and each state (quenched or unquenched). The model for the simultaneous target analysis now reads

$$\begin{bmatrix} \Psi_{U,590} \\ \Psi_{Q,590} \\ \Psi_{U,400} \\ \Psi_{Q,400} \end{bmatrix} = \begin{bmatrix} C_{U,590} \\ \alpha_1 C_{Q,590} \\ \alpha_2 C_{U,400} \\ \alpha_3 C_{Q,400} \end{bmatrix} SAS^T$$

where Ψ indicates the data measured in each of the four experiments (U or Q, with 400 or 590 nm excitation) and the α_i are the three relative scaling parameters. All unknown parameters (kinetic, input or SAS) are now estimated with the help of the partitioned variable projection algorithm (van Stokkum, Larsen et al. 2004; Mullen and van Stokkum 2009). Furthermore, after convergence, the linear approximation covariance matrix allows us to estimate the precision of the estimated parameters. With the good quality of fit (see below) the relative precision of the estimated parameters was better than 10%, with the exception of the rates that describe the fast energy transfer between APC₆₈₀ and PS II or PS I bulk.

Quality of the fit

The parameter estimation resulted in parameters that describe the model fit to the data, and the corresponding residuals. The rmse of the fit was 1.69, which is less than 1% of the maximum of most of the traces in Fig.SI.3 (the absolute maximum of these data was 575 at 647 nm). In addition, for each of the four experiments the matrix of residuals was analysed by Singular Value Decomposition (van Stokkum, van Oort et al. 2008). This enabled us to spot trends in the residuals and locate the lack of fit in the time or wavelength domain. The left singular vectors in Fig.SI.4a,c indicate that the maximum lack of fit is around the IRF maximum. This indicates that the fit can be further improved by a more flexible IRF description.

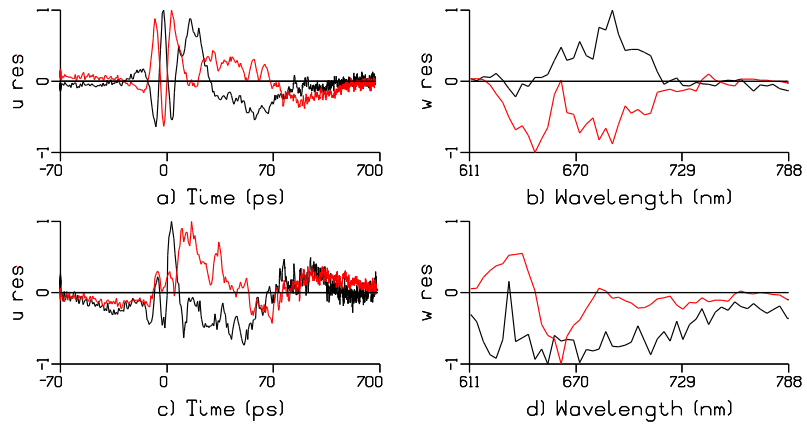


Fig.SI.4 First left (a,c) and right (b,d) singular vectors resulting from Singular Value Decomposition of the matrix of residuals of the four OverOCP experiments fitted in Fig.SI.3. Key: unquenched 400 (black in a,b), quenched 400 (red in a,b) unquenched 590 (black in c,d), quenched 590 (red in c,d) nm excitation. Note that the time axis in (a,c) is linear until 70 ps and logarithmic thereafter.

| identity | loose PS I | loose PS II | PSII_PBS | PSI_PBS | total PS II | total PS I | PS I/II ratio | PBS_Q | PBS_NQ | PBS_tot | total | PS II | PS I | PBS |
|-------------------|-------------------|------------------|----------|---------|----------------|---------------|------------------|-------|--------|--------------------|-------|-------|-------|-------|
| U over 590 exc | 16.7 ^a | 2.3 ^b | 0.5 | 1.5 | 2.8 | 18.2 | 6.5 | 107.5 | 42.5 | 150.0 ^c | 171.0 | 1.6% | 10.6% | 87.7% |
| Q over 590 exc | 16.7 | 2.3 | 0.5 | 1.5 | 2.8 | 18.2 | 6.5 | 107.5 | 42.5 | 150.0 | 171.0 | 1.6% | 10.6% | 87.7% |
| U over 400 exc | 199.8 | 27.6 | 6.0 | 18.0 | 33.6 | 217.8 | 6.5 | 13.2 | 5.2 | 18.4 ^d | 269.8 | 12.4% | 80.7% | 6.8% |
| Q over 400 exc | 199.8 | 27.6 | 6.0 | 18.0 | 33.6 | 217.8 | 6.5 | 13.2 | 5.2 | 18.4 | 269.8 | 12.4% | 80.7% | 6.8% |
| | | | | | | | | | | | | | | |
| U WT 590 exc | 16.7 | 2.3 | 0.5 | 1.5 | 2.8 | 18.2 | 6.5 | 41.6 | 108.4 | 150.0 | 171.0 | 1.6% | 10.6% | 87.7% |
| Q WT 590 exc | 16.7 | 2.3 | 0.5 | 1.5 | 2.8 | 18.2 | 6.5 | 41.6 | 108.4 | 150.0 | 171.0 | 1.6% | 10.6% | 87.7% |
| U WT 400 exc | 199.8 | 27.6 | 6.0 | 18.0 | 33.6 | 217.8 | 6.5 | 6.4 | 16.8 | 23.2 | 274.6 | 12.2% | 79.3% | 8.5% |
| Q WT 400 exc | 199.8 | 27.6 | 6.0 | 18.0 | 33.6 | 217.8 | 6.5 | 6.4 | 16.8 | 23.2 | 274.6 | 12.2% | 79.3% | 8.5% |

a. Parameter $l1_{590}$

b. Parameter $l2_{590}$

c. Parameter $\mathcal{E}C_{590}$

d. Parameter $\mathcal{E}C_{400}$

Table SI.1 Input values for target analysis of OverOCP and WT, and derived numbers: fraction excited PBS, PS I, PS II and PS I/II ratio.
Footnotes refer to parameters of Table SI.2

With 590 nm excitation we excite about 88% PBs, and 12% photosystems. Conversely, with 400 nm excitation we excite 6.8% and 8.5% PBs for OverOCP and WT respectively, and 93.2 (91.5) % photosystems. Both are in accordance with the literature (Krumova, Laptenok et al. 2010). The PS I/II ratio is about 6.5 on a Chl basis.

The estimated parameters are shown in Fig.SI.2 (rate constants), Fig.SI.5 (SAS), Table SI.1 (input parameters) and Table SI.2 (absorption and quenching parameters). Most of the rate constants can be estimated with a relative precision of about 10%, except for the fastest rates that describe the coupling of APC₆₈₀ and PSII or PSIb. These rates are most probably too fast to be resolved precisely with the present experiments. As a consequence, also the APC₆₈₀ SAS is estimated less precisely than the other six SAS.

Table SI.2 Quenching and absorption parameters (note that by definition $\varepsilon 2_{590} \equiv 1$). For definitions see text.

| | k_Q (1/ns) | q | $\varepsilon 2_{400}$ | εc_{590} | εc_{400} |
|----------|--------------|-----|-----------------------|-----------------------|-----------------------|
| Over_OCP | 66 | 72% | 12 | 150 | 18.4 |
| WT | 54 | 29% | 12 | 150 | 23.2 |

According to the fitting results, about 72% of the PBs appeared to be quenched for Over_OCP, whereas for WT the fraction q was only about 29%. In the quenched PBs, the quenching rate of the APC₆₆₀ compartment was about 66/ns. The value of 12 for parameter $\varepsilon 2_{400}$ corresponds in Fig.SI.6G to a ratio of 12 for the amplitudes of the dashed and solid concentration profiles.

The plausibility of the estimated parameters was judged by the following criteria: realistic shapes of the estimated SAS, and realistic areas of the SAS in accordance with literature (Cohen-Bazire, Beguin et al. 1977; Porra, Thompson et al. 1989; Debreczeny, Sauer et al. 1995). We aimed for approximately equal areas of the four PB SAS, and equal areas of the PSII, PSIb, PSIr SAS. The area of a PS SAS relative to that of a PB SAS was taken to be about 0.6. The lifetimes calculated from the estimated rate constants of the energy funnel PC-S, PC-L, APC₆₆₀, APC₆₈₀ and of PSI are globally in accordance with previous experimental results presented in literature (Bittersmann and Vermaas 1991; Gobets, van Stokkum et al. 2001).

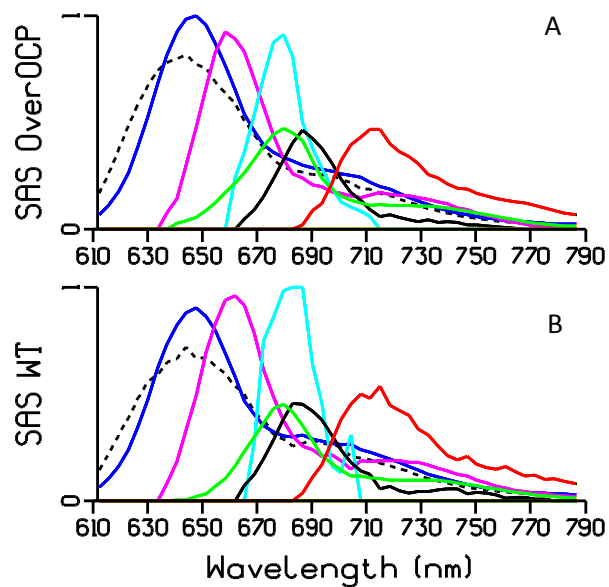


Fig.SI.5 SAS estimated from the target analysis using the kinetic scheme in Fig.SI.2. Key: PC-S (black dash), PC-L (blue), APC₆₆₀ (magenta), APC₆₈₀ (cyan), PS II (green), PS I bulk (black), PS I red (red). (A) OverOCP, (B) WT.

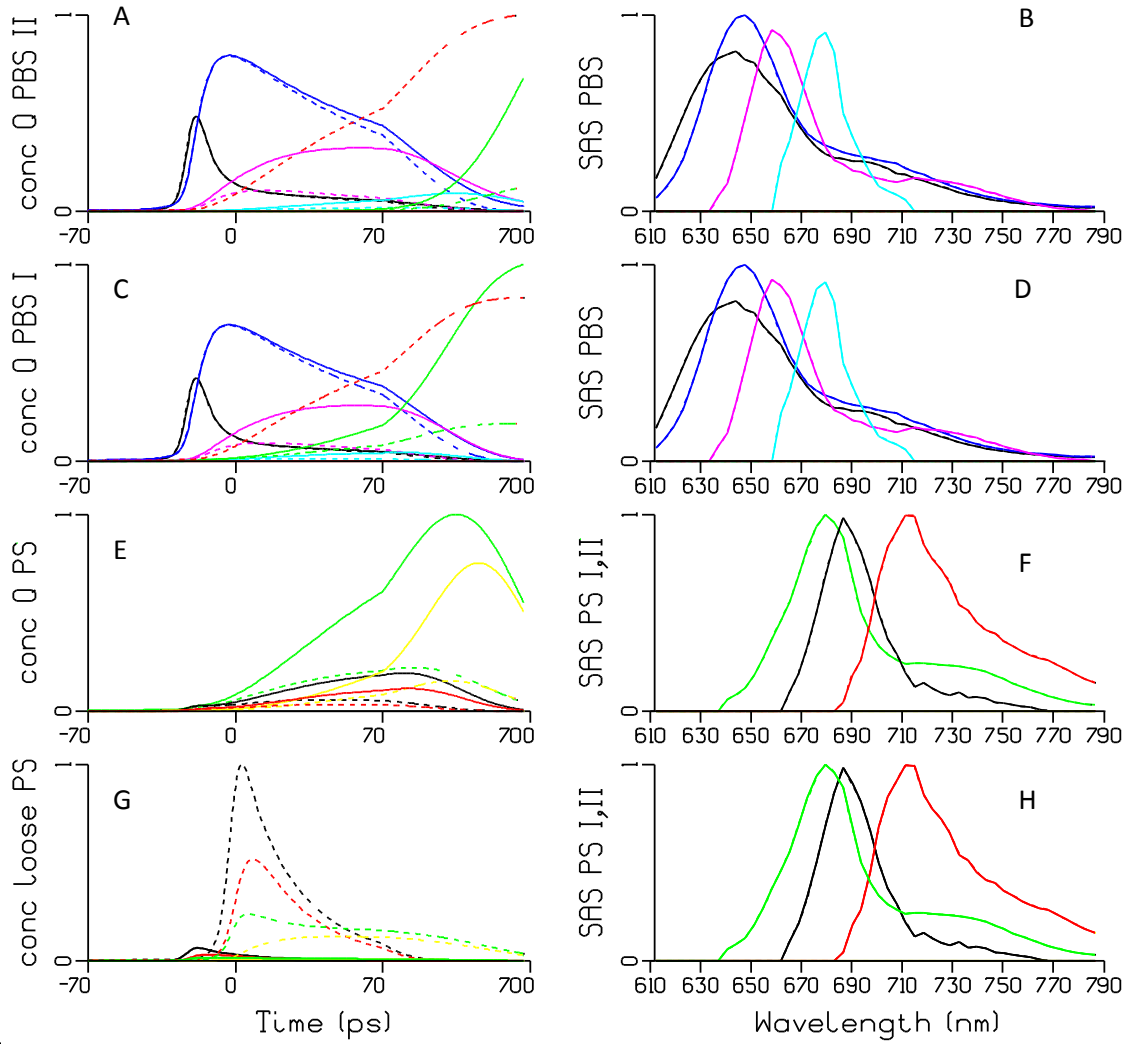


Fig.SI.6 Concentration profiles (left hand column) and SAS (right hand column) estimated from the target analysis of OverOCP using the kinetic scheme of Fig.SI.2. The PBs in panels A and C are connected to PSII and PSI, respectively. In (A,C,E) solid and dashed indicate concentrations for the unquenched and quenched case, respectively. Key to A-D: PC-S (black), PC-L (blue), APC₆₆₀ (magenta), APC₆₈₀ (cyan), integrated nonphotochemical quenching (red), integrated photochemical quenching (green). Key to E-H: PS II (green), PS I bulk (black), PS I red (red in E-G) and NonRadiative (yellow). In (G) solid and dashed indicate 590 and 400 nm excitation, respectively. Note that the time axis is linear until 70 ps, and logarithmic thereafter.

The quenching mechanism is further illustrated in Fig.SI.6. The solid lines in panels A,C,E reflect the unquenched situation, where the equilibria cause multiexponential decay kinetics for all concentration profiles. Panels A,B depict the energy funnel PC-S, PC-L, APC₆₆₀, APC₆₈₀; for clarity the information of the attached PSII has been omitted here. Panels C,D visualize the quenching of PB coupled to PSI. Note that the difference between panels A and C is visible as a small, long lasting emission which can be attributed to the equilibrium of PBs and the partially closed PSII RCs. Most important is the concentration of the quenched excitations. The integrated

nonphotochemical quenching is indicated in dashed red, whereas the integrated *photochemical* quenching is depicted in green in A,C. In the computation of *photochemical* quenching in the partially closed PSII RC we have integrated all excitations that decay via the NR compartment. The solid green is the *photochemical* quenching in unquenched conditions, note that this rises quickly for PSI, whereas for PSII it rises slowly because of the equilibrium and long lifetimes. The dashed green represents the photosystems with quenched PB. Clearly, the yield of photosynthesis is reduced by more than 80%. In the quenched PB, the dashed lines show the largest differences for APC₆₆₀, and of course also for APC₆₈₀ which receives its input from APC₆₆₀. In the photosystems that are in turn coupled to APC₆₈₀ the same non-photochemical quenching is visible in panels E,F as a large difference between the solid and dashed lines. The dynamics of the photosystems without PB is visible in panels G,H. The PSIb, PSIr equilibrium is established in about 4 ps, and after this the equilibrated PSI decays in about 28 ps by charge separation (photochemical quenching). These *in vivo* results are in agreement with the properties of cyanobacterial PSI *in vitro* (Gobets and van Grondelle 2001; Gobets, van Stokkum et al. 2001) and *in vivo* (Krumova et al. 2010). Finally, PSII equilibrates with the NR compartment in about 45 ps, which is in accordance with the observed lifetime (dominantly 49 ps) for primary charge separation in PSII core (Miloslavina, Szczeplaniak et al. 2006; van der Weij-de Wit, Dekker et al. 2011). Thereafter, the equilibrated PSII decays slowly with 354 ps. The large amplitude of this slow decay component indicates that the PSII RC is partially closed.

Reconstruction of the steady-state spectra

The results from the target analysis can be used to predict the contributions of each of the SAS to the steady-state spectrum. We used the estimated input and kinetic parameters of OverOCP with 590 nm excitation to compute the steady-state concentration of each of the species. The kinetic scheme of Figure SI.2 results in concentrations of each compartment described by six (PSII, PSI coupled to PBs quenched or unquenched) or two (loose PSII, PSI) exponential decays. Then the concentration of each compartment was integrated over time, and the contributions of all compartments belonging to a species were summed. Thus we arrived at the amplitudes of the SAS contributions depicted in Figure SI.7A and B. The sum of all these contributions is the reconstructed steady-state spectrum in the unquenched (A) or quenched (B) state. The agreement with the measured steady-state spectra of Figure 2B is considered good. Thus we have explained both the change in shape and in amplitude of Figure 2B.

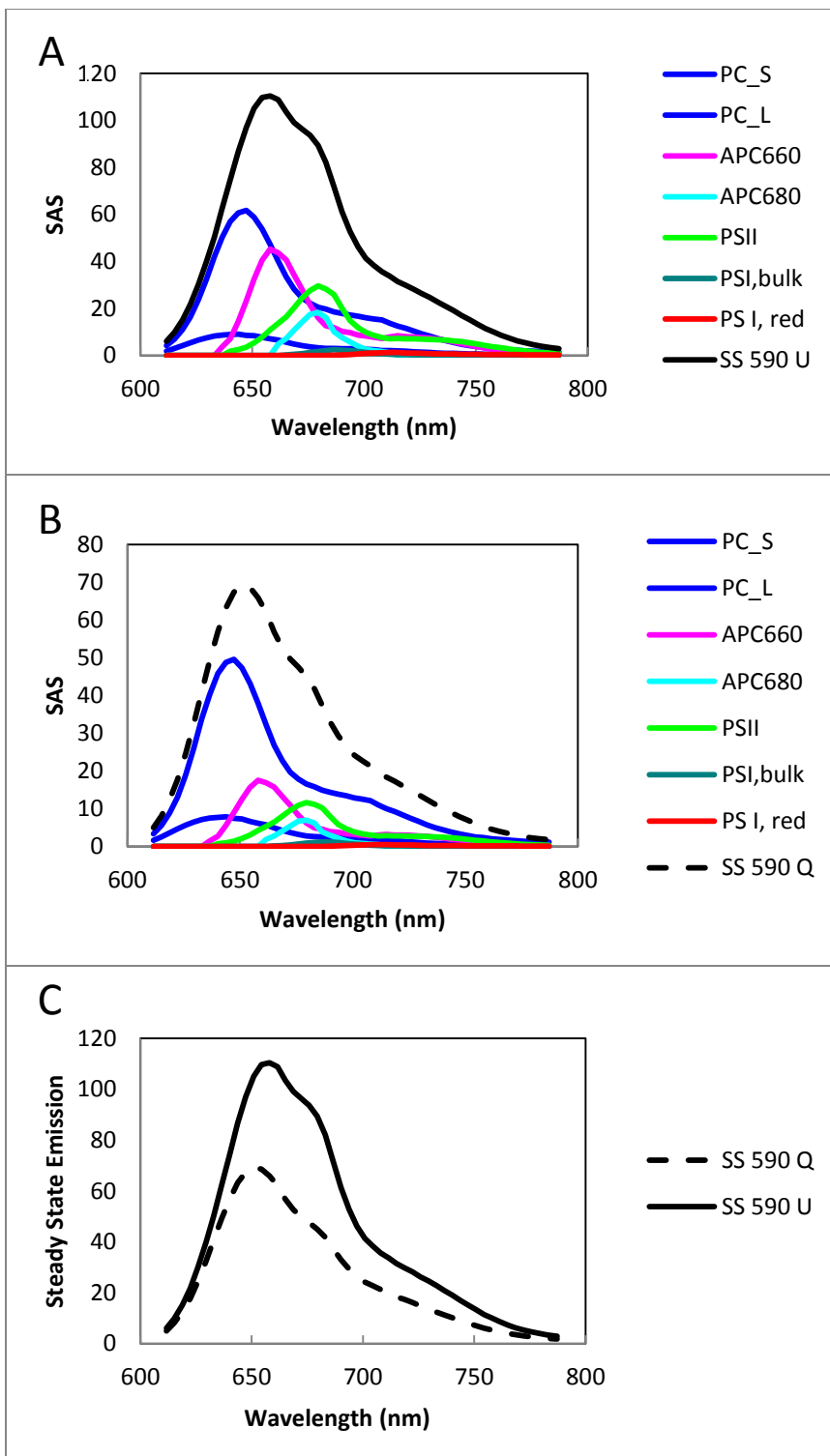


Fig.SI.7 Reconstructed steady-state spectra of OverOCP with 590 nm excitation in the unquenched and quenched state using the kinetic scheme of Fig.SI.2 and the inputs of Table SI.1. In panels A and B, spectral contributions of each species are shown. The black curves represent the sum of these for the unquenched (solid) and quenched (dash) state, and are shown again in panel C.

WT target analysis

The four WT experiments have been subjected to target analysis analogously to the four OverOCP experiments. For comparison, the estimated quenching and input parameters have been added to Table SI.1 and SI.2. The estimated quenching fraction was 29%, and the quenching rate was 54/ns. This value agrees with the more precise value of $kQ = (66 \pm 15) / ns$ that was determined from the OverOCP experiments. The estimated SAS are depicted in Fig.SI5B. These WT SAS agree well with the OverOCP SAS of Fig.SI5A. The largest differences are present for the APC₆₈₀SAS (cyan), which is the most difficult one to resolve. The estimated rate constants differ from those in Figure SI.2 mainly for the description of the equilibrium within PSII, which indicates variation in the fraction of closed PSIIRCs.

References

- Ashby, M. K. and C. W. Mullineaux (1999). "The role of ApcD and ApcF in energy transfer from phycobilisomes to PSI and PSII in a cyanobacterium." *Photosynthesis Research* **61**(2): 169-179.
- Bittersmann, E. and W. Vermaas (1991). "Fluorescence Lifetime Studies of Cyanobacterial Photosystem-II Mutants." *Biochimica Et Biophysica Acta* **1098**(1): 105-116.
- Cohen-Bazire, G., S. Beguin, et al. (1977). "Physico-chemical and immunological properties of allophycocyanins." *Arch Microbiol* **111**(3): 225-238.
- Debreczeny, M. P., K. Sauer, et al. (1995). "Comparison of Calculated and Experimentally Resolved Rate Constants for Excitation-Energy Transfer in C-Phycocyanin .1. Monomers." *Journal of Physical Chemistry* **99**(20): 8412-8419.
- Dong, C., A. Tang, et al. (2009). "ApcD is necessary for efficient energy transfer from phycobilisomes to photosystem I and helps to prevent photoinhibition in the cyanobacterium Synechococcus sp. PCC 7002." *Biochimica et Biophysica Acta (BBA) - Bioenergetics* **1787**(9): 1122-1128.
- Gobets, B. and R. van Grondelle (2001). "Energy transfer and trapping in photosystem I." *Biochimica Et Biophysica Acta-Bioenergetics* **1507**(1-3): 80-99.
- Gobets, B., I. H. M. van Stokkum, et al. (2001). "Time-resolved fluorescence emission measurements of photosystem I particles of various cyanobacteria: A unified compartmental model." *Biophysical Journal* **81**(1): 407-424.
- Kirillovsky, D. and C. A. Kerfeld (2011). "The orange carotenoid protein in photoprotection of photosystem II in cyanobacteria." *Biochimica Et Biophysica Acta*.
- Krumova, S. B., S. P. Laptenok, et al. (2010). "Monitoring Photosynthesis in Individual Cells of Synechocystis sp. PCC 6803 on a Picosecond Timescale." *Biophysical Journal* **99**(6): 2006-2015.
- Miloslavina, Y., M. Szczepaniak, et al. (2006). "Charge separation kinetics in intact photosystem II core particles is trap-limited. A picosecond fluorescence study." *Biochemistry* **45**(7): 2436-2442.
- Mullen, K. M. and I. H. M. van Stokkum (2009). "The variable projection algorithm in time-resolved spectroscopy, microscopy and mass spectrometry applications." *Numerical Algorithms* **51**(3): 319-340.
- Ohki, K., Y. Okabe, et al. (1987). "A Comparative-Study of Quantitative Relationship between Phycobiliproteins and Photosystem-II in Cyanobacteria and Red Algae." *Plant and Cell Physiology* **28**(7): 1219-1226.
- Porra, R. J., W. A. Thompson, et al. (1989). "Determination of Accurate Extinction Coefficients and Simultaneous-Equations for Assaying Chlorophyll-a and Chlorophyll-B Extracted with 4 Different Solvents - Verification of the Concentration of Chlorophyll Standards by Atomic-Absorption Spectroscopy." *Biochimica Et Biophysica Acta* **975**(3): 384-394.

- van der Weij-de Wit, C. D., J. P. Dekker, et al. (2011). "Charge Separation is Virtually Irreversible in Photosystem II Core Complexes with Oxidized Primary Quinone Acceptor." The Journal of Physical Chemistry A: null-null.
- van Stokkum, I. H. M., D. S. Larsen, et al. (2004). "Global and target analysis of time-resolved spectra." Biochimica Et Biophysica Acta-Bioenergetics **1657**(2-3): 82-104.
- van Stokkum, I. H. M., B. van Oort, et al. (2008). (Sub)-Picosecond Spectral Evolution of Fluorescence Studied with a Synchroscan Streak-Camera System and Target Analysis. Biophysical Techniques in Photosynthesis Vol. II. T. J. Aartsma and J. Matysik. Dordrecht, The Netherlands, Springer: 223-240.